Citation for final published version:

Rabizadeh, Taher, Stawski, Tomasz M., Morgan, David John , Peacock, Caroline L. and Benning, Liane G. 2017. The effects of inorganic additives on the nucleation and growth kinetics of calcium sulfate dihydrate crystals. Crystal Growth and Design 17 (2) , pp. 582-589. 10.1021/acs.cgd.6b01441

Publishers page: http://dx.doi.org/10.1021/acs.cgd.6b01441

The effects of inorganic additives on the nucleation and growth kinetics of calcium sulfate dihydrate crystals

Taher Rabizadeh[1*], Tomasz M. Stawski [2], David J. Morgan[4], Caroline L. Peacock[1], Liane G. Benning[1,2,3*]

1- Cohen Geochemistry Laboratory, School of Earth and Environment, University of Leeds, Leeds, LS2 9JT, United Kingdom

2- GFZ, German Research Centre for Geosciences, Telegrafenberg, 14473 Potsdam, Germany

3- Department of Earth Sciences, Free University of Berlin, 12249 Berlin, Germany

4- Cardiff Catalysis Institute, School of Chemistry, Cardiff University, Cardiff, CF10 3AT, United Kingdom

* Correspondence to: Taher Rabizadeh (eetr@leeds.ac.uk) and Liane G. Benning (Benning@gfz-potsdam.de)

Abstract

The effects of 50-500 mmol/L alkali and alkaline earth metal additives (Li^+, Na^+, K^+, Mg^{2+}) on the crystallisation kinetics and mechanisms of calcium sulfate dihydrate (gypsum; $CaSO_4 \cdot 2H_2O$) from supersaturated aqueous solutions were determined by *in situ* and time resolved UV-VIS spectrophotometry. The surface or structural associations between these additives and the end-product gypsum crystals were evaluated through a combination of inductively coupled plasma mass or optical emission spectrometric analyses of digested end-products and X-ray photoelectron spectroscopy (XPS) of the surface composition of the solids. Furthermore, X-ray diffraction (XRD) and scanning electron microscopy (SEM) were utilised for determining any changes in phase composition and morphologies of the formed crystals. Our results revealed that Mg^{2+}, even at low concentrations, decreased the nucleation and growth kinetics 5-10 fold more than Li^+, Na^+ and K^+. In all cases, the additives also changed the shapes and sizes of the formed crystals, with Mg^{2+} and Li^+ resulting in longer and thinner crystals compared to the additive-free system. In addition, we showed that, regardless of concentration, Mg^{2+}, Li^+ and K^+ only adsorbed to the newly forming surfaces of the growing gypsum crystals, while ~ 25% of Na^+ became incorporated into the synthesised crystals.

Keywords: crystallisation; calcium sulfate dihydrate; kinetics, surface adsorption; X-ray photoelectron spectroscopy

1. Introduction

Calcium sulfate dihydrate is one of the main evaporite minerals at Earth surface conditions (Freyer & Voigt, 2003) and it is a crucial mineral phase in many industrial processes, where it is extensively used for construction, medical or agricultural applications (Guan, Ma et al., 2009; Ossario et al., 2014). However, in several industrial processes that rely on water handling systems (e.g., oil and gas production, water desalination; Moghaddasi et al., 2006; Rahardianto et al., 2008), the precipitation of gypsum from the fluids results in its deposition as mineral scales on pipes, filters and heat exchangers. This leads to increased cost and reduction in production efficiency. Thus, it is paramount to quantitatively understand how gypsum forms in such systems, particularly because the effects that aqueous ions present in, for example, formation waters, may have on the crystallisation kinetics and morphology of gypsum are still poorly understood. It is well known that both inorganic (Akyol et al., 2009) and organic additives (e.g., Hoang et al., 2011; Rabizadeh et al., 2014) affect the nucleation, crystallisation and morphologies of gypsum crystals. To date primarily the role that trace elements like Cr^{3+}, Cu^{3+}, Al^{3+} and Fe^{3+} have on gypsum growth from solution Hamdona and Al Hadad, 2007; Hasson et al., 1990; Kruger et al., 2001; Sayan et al., 2007; Yang et al., 2009 have been studied. In contrast, the effect of major ions in, for example, brines or formation water fluids (e.g., Na^+, K^+, Li^+, Cl^- or Mg^{2+}) are far less understood. Furthermore, existing data from studies that address the crystallisation of calcium sulfate phases in the presence of these ions are highly discrepant and whether these ions become structurally incorporated or only surface adsorbed into the growing gypsum is still debated. For example, Na^+ has been shown to incorporate into the calcium sulphate hemihydrate ($CaSO_4$ 0.5 H_2O; bassanite; Mao et al., 2014) but not into gypsum (Ben Ahmed et al., 2014). On the other hand, Mg^{2+} was suggested to only incorporate into gypsum (Ben Ahmed et al., 2014). However, lacking so far is a quantitative and molecular lavel understanding of the processes that lead either to these ions becoming adsorbed onto or incorporated into growing gypsum crystal structures. Lacking is also a mechanistic pathway explaining the role that these crucial ions in brines have on the nucleation, growth and crystallisation of gypsum.

To fill this gap we have in this work elucidated the effects that variable concentrations (0-500 mmol/L) of aqueous Li^+, Na^+, K^+ and Mg^{2+} ions have on the nucleation and growth kinetics, as well as the morphology of gypsum forming from supersaturated aqueous solutions. We followed the processes by combining analyses of the solution and solids. We determined the mechanisms that control the way these alkali and alkaline earth cations became associated with growing gypsum crystals. We show, in contrast with previously published data, that Li^+, K^+ and Mg^{2+} do not incorporate at all into the forming gypsum structures while Na^+ became partly incorporated but still the majority became adsorbed to growing gypsum crystals. However, the major effect that all ions have is in delaying the nucleation and growth through adsorption onto the growing mineral surfaces. In the case of Mg^{2+} and Li^{+} this interaction also leads to a change in the resulting crystal morphologies.

2. Experimental methods

Calcium and sulfate stock solutions were prepared from dissolving analytical grade $CaCl_2 \cdot 2H_2O$ (≥99-100%; AnalaR Normapour; VWR) and diluting concentrated H_2SO_4 (93-98% v/vol, AnalaR Normapour; VWR) in 18 MΩcm^{-1} ultra-pure Milli-Q water to reach concentrations of 200 mmol/L. The effects of inorganic metal ions on gypsum crystallisation were evaluated by adding Li^{+}, Na^{+}, K^{+} and Mg^{2+} to separate $CaCl_2 \cdot 2H_2O$ stock solutions, using analytical grade LiCl (puriss. p.a., anhydrous, ≥99.0%; Sigma-Aldrich), NaCl (≥99.9%; Fisher), KCl (puriss. p.a., anhydrous, ≥99-100%; Sigma-Aldrich) and $MgCl_2.6H_2O$ (≥99-100%; AnalaR Normapour; VWR). Precipitates were produced by mixing 1 ml of $CaCl_2 \cdot 2H_2O$ with or without the additives with 1 ml H_2SO_4 in 4 ml polystyrene cuvettes at room temperature (21 °C) and under constant stirring. The mixing led to a solution with a pH of ~ 2 and initial $[Ca^{2+}]$ and $[SO_4^{2-}]$ concentrations of 100 mmol/L. The initial concentration of additives in the crystallisation solutions (after mixing) was varied between 50 and 500 mmol/L. Once mixed, all solutions were supersaturated with respect to gypsum as indicated by the saturation indices (as the logarithm of the ion activity product over the solubility product) calculated with the geochemical computer code PhreeqC 3.3.3 and using the PITZER database (Parkhurst and Appelo, 1999).

Changes in the mixed solutions were monitored by measuring the increase in absorbance using a UV-VIS spectrophotometer (Uvikon XL) at $\lambda = 520$ nm with an angle between the incident beam and detector of 180°. The reactions were followed at room temperature for up to 200 minutes with UV-VIS data collected every second and each experimental set was carried out in triplicate. The absorbance data is plotted as the normalized change in solution turbidity. At the end of each turbidity experiment, the contents of each cuvette were vacuum filtered through 0.2 μm polycarbonate filters, dried and preserved for further analyses (for additional details see Supplementary information Fig. S1).

In all experiments, regardless if additives were present or not, the solid end-products were always gypsum as determined by powder X-ray diffraction (XRD; Bruker D8 diffractometer; CuKα1; 2θ range 5 - 35°; resolution 0.105° / step; counting time 1s / step) with XRD patterns analysed with the EVA software (version 3) and the PDF-2-1996 database (see Fig. S2). To accurately determine the d-spacing in all samples, each gypsum end-product powder was mixed with a silicon standard reference material prior to XRD analysis.

The morphologies of the resulting gypsum crystals were imaged using a field emission gun scanning electron microscope (FEG-SEM, FEI Quanta 650, 5 kV) and the dimensions of the crystals were evaluated by measuring the lengths and widths of 200 crystals in each sample using the ImageJ v. 1.49 software Abràmoff et al., 2004.

To evaluate the association between the additives and the formed gypsum, aliquots of the precipitated end-products were dissolved in 2% nitric acid (69% AnalaR NORMAPUR analytical reagent) and the resulting solutions analysed for their Na, Mg, Li, K and Ca contents by inductively coupled plasma mass spectrometry (ICP-MS; Thermo Scientific iCAPQc) and inductively coupled plasma optical emission spectrometer (ICP-OES; Thermo Scientific iCAP 7400); for limit of detection and uncertainties see table S1). To differentiate between the potentially surface adsorbed and the structurally incorporated fractions of the additives, aliquots of the end-product gypsum samples were first rinsed 6 times with a saturated gypsum solution to desorb any potentially surface adsorbed additives. The saturated gypsum solution was prepared by equilibrating gypsum (puriss, 99.0-101.0%, Sigma-Aldrich) in 18 MΩcm^{-1} ultra-pure Milli-Q water at pH 2 for 24 hours and filtering through 0.2 μm syringe filters prior to desorption. After this desorption step the remaining solids were digested in 2% nitric acid and the digestion solutions were analysed as described above. The concentrations of additives associated with the end-product gypsum crystals (association amount; C_A) before and after desorption were calculated from the moles of cation measured in the full digestion solution divided by the moles of total dissolved gypsum crystals.

Finally, to determine the nature of the surface interactions between the various ions and the formed precipitates, we employed X-ray photoelectron spectroscopy (XPS) with a detection limit of 0.1 at.% (which is roughly 1ppth or 10^{19} atoms/cm^3). On both the as-formed and the desorbed end-product solids, XPS was used to determine whether and how metal ions were associated with the mineral surfaces or the crystal structures. XPS spectra were acquired from the top 8-10 nm of end-product gypsum crystals using a Kratos Axis Ultra-DLD spectrometer with a monochromatic Al K_α X-ray source (144 W) and analyser pass energies of either 160 eV (survey scans) or 40 eV (high resolution scans). The base pressure during analysis was ca. 5×10^{-9} Torr. All data were referenced to the C (1s) signal of adventitious carbon at 284.8 eV and quantified as atomic percentage using CasaXPS^{TM} (Version 2.3.15) using elemental sensitivity factors supplied by the manufacturer.

3. Results

3.1. The effects of additives on the crystallisation process

In the additive-free experiments, the turbidity started to develop after 3±1 minutes (induction time) and it took ~ 30 minutes for the turbidity to reach a steady value on a plateau (Fig 1a, black line). In contrast, in each of the additive-containing experiments (Fig. 1a and b), the induction times and the time to reach a plateau were markedly longer. At the highest concentration (500 mmol/L) of monovalent cations (Li^+, Na^+ and K^+), the induction time increased in the order $K^+ < Na^+ < Li^+$ by 2 fold, 4 fold and almost 5 fold, respectively (Table S2). The slope of the turbidity decreased and the crystallisation end-plateaus were reached significantly later than in the additive free system in the same order (K^+ ~ 37 min, Na^+ ~ 48 min and Li^+ ~ 60 min; Fig. 1a). The turbidity development was even more affected by the presences of Mg^{2+}. Even at a low additive concentration (e.g., 100 mmol/L; Fig 1a) the induction time much longer than for all monovalent cations at 500 mmol/L. Quadrupling the Mg^{2+} concentration from 50 mmol/L to 200 mmol/L, increased the induction time exponentially; Fig. 1b, Table S2). Furthermore, for Mg^{2+} at 300 and 500 mmol/L even after 200 minutes of reaction no change in turbidity was observed indicating total inhibition of the reaction under these experimental conditions. For all additives with increasing cation concentrations the induction time increased in linearly (Fig. 1c), but the effect was markedly larger for the divalent Mg^{2+} compared to the monovalent Li^+, Na^+ and K^+ (Fig. 1c).

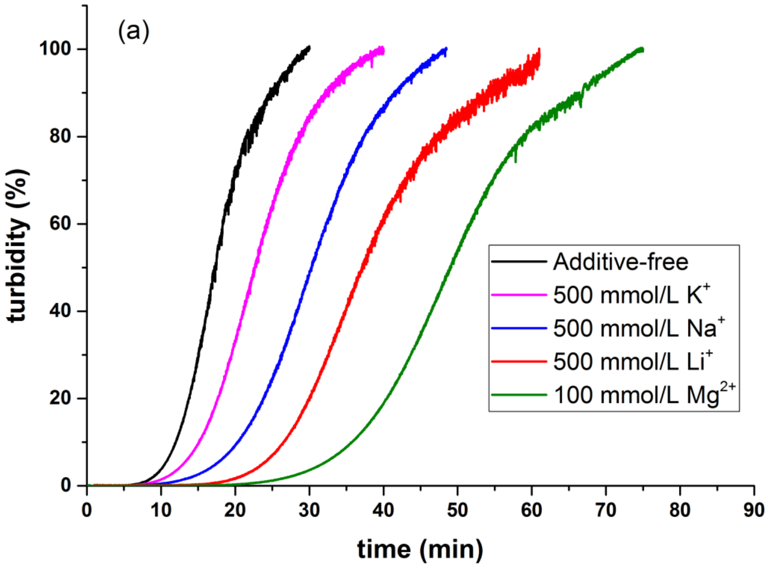

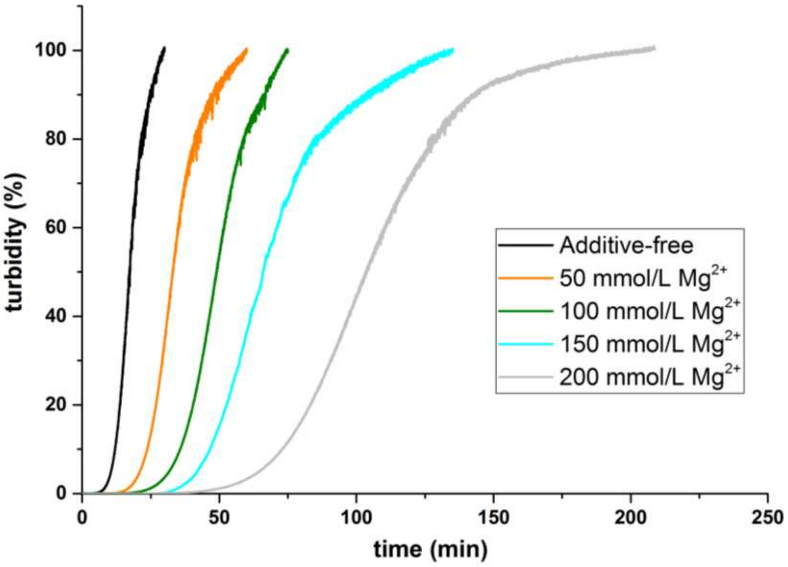

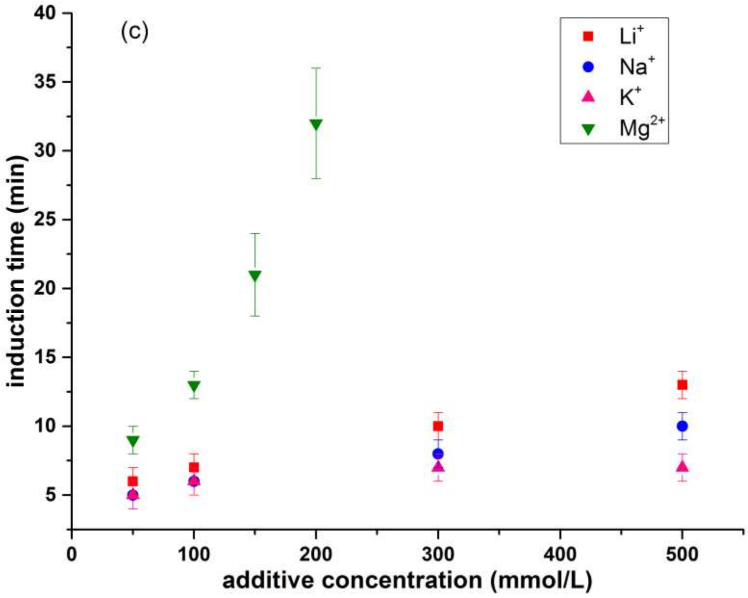

Fig. 1. Turbidity curves plotted as a function of time (a) in the absence and presence of high concentrations of additives (note that Mg^{2+} is only 100 mmol/L while all monovalent ions are 500 mmol/l) ; (b) at variable concentrations of Mg^{2+}; (c) changes in induction times as a function of additive concentrations.

3.2 The association between additives and gypsum crystals

For all additive ions, increasing additive concentration in solution was mirrored by an increase in associated ion concentration (C_A) in the solids formed (Fig. 2a-d). For example, for monovalent additive concentrations between 50 and 500 mmol/L, $C_{A\,Li^+}$increased ~ 5 times, while $C_{A\,Na^+}$ and $C_{A\,K^+}$ increased ~ 3 times (Fig. 2a-c). For Mg^{2+} at concentrations up to 200 mmol/L, the $C_{A\,Mg^{2+}}$ increased ~ 4 times (Fig. 2d) and reached a value almost equivalent to the highest value obtained for the C_A of Li^+ at 500 mmol/l. Comparing the association amounts at a fixed additive concentration (100 mmol/L), mirrors the trend observed for the increase in induction time, namely $K^+ < Na^+ < Li^+ < Mg^{2+}$.

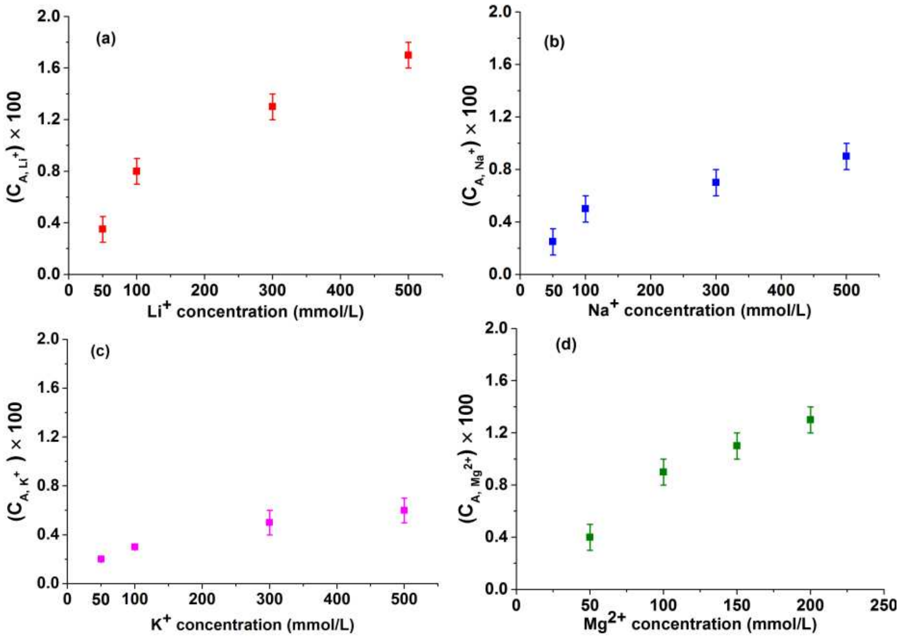

Fig. 2. Variations in cation association at different concentrations of (a) Li^+ (b) Na^+ (c) K^+ (d) Mg^{2+}; the error bars represent the standard deviations measured in five replicate samples.

When we evaluated the partitioning of additives between crystal surfaces (adsorption) or crystal matrixes (structural incorporation), our data revealed that the C_A for Li^+, K^+ and Mg^{2+} in the post desorption digested samples were below detection limits. This clearly indicated that these cations were only adsorbed to the surfaces of the growing gypsum crystals with insignificant or no incorporation into the crystal structures. In contrast, at the highest additive concentrations (500 mmol/L), up to 25% of the associated Na^+ ($C_{A\ 500mmol/L}$ = 0.002 out of 0.009) became incorporated into the gypsum structure (Fig S3). The additive ion adsorption was also confirmed by XPS surface analyses of as-formed and desorbed gypsum crystals (Fig. 3) The XPS spectra confirmed that the Li 1s (55.8 eV), K $2p_{3/2}$ (292.9 eV) and Mg 2s (89.8 eV) peaks were present in all as-formed samples but absent in the post-desorbed samples confirming that these ions were solely surface adsorbed and not incorporated into the gypsum structure (Fig. 3a, c and d). On the other hand, for Na^+ the 1s peak at 1071.64 eV was present in both the as-formed and desorbed gypsum spectra, again corroborating our C_A data (Fig. 3b) that a fraction of the associated Na^+ became sequestered into the gypsum crystal structure. The surface elemental compositions (in atomic percentage) of the as-produced and desorbed gypsum crystals illustrated that Li^+ had the adsorption affinity (1.52 at. %) followed by Mg^{2+} (1.06 at. %), Na^+ (0.34 at. %) and K^+ (0.41 at. %) (Table 1). However, unlike Li^+, K^+ and Mg^{2+}, Na^+ remained associated with the gypsum crystals post desorption (0.14 at. %) confirming its structural incorporation. Note the signal of lithium is low due to the small ionisation cross-section of the metal, however the presence of Li can be detected by subtraction of the satellite structure noted in fig 3.

Commented [DM1]: Only quote to 1dp as we used 0.1 eV steps

Commented [DM2]: What do we know about the dispersion of these elements? XPS concentrations can be influenced by dispersion – e.g. the smaller the particles and more well dispersed they are then the higher the apparent concentration

Together with the adsorbed ions, in all as-formed but not the desorbed samples, the XPS spectra revealed the presence of Cl^- $2p_{3/2}$ peaks confirming that Cl^- also became co-adsorbed to the gypsum surfaces (Fig. S4). Furthermore, the Ca to S atomic % ratio was close to 1:1 but the O to Ca or S ratio was higher than 4:1, likely related to gypsum structural water (Table 1).

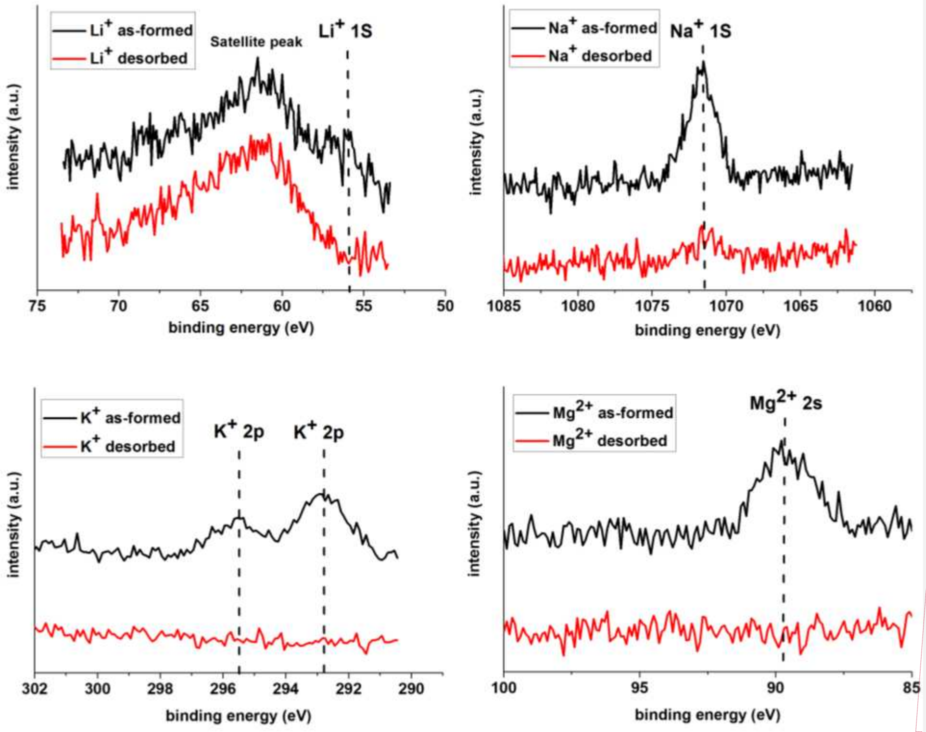

Fig. 3. XPS spectra for the as-formed and desorbed gypsum crystals containing additive cations. Note that the peak intensities are in arbitrary units and do not represent the concentration of the elements on the surface.

Commented [DM3]: Make swure the S of 1S, P of 2p etc is lowercase

Table 1. Surface composition of the precipitated gypsum crystals detected by XPS (at. %)

Commented [DM4]: Again quote to 1dp concentration wise

	Ca	S	O	Li	Na	K	Mg	Cl	C
Additive-free (as-formed)	11.51	12.01	58.34	-	-	-	-	-	18.14
Additive-free (desorbed)	11.56	12.04	58.29	-	-	-	-	-	18.12
Li$^+$-500 mmol/L (as-formed)	9.59	9.98	52.34	1.52	-	-	-	1.77	24.80
Li$^+$-500 mmol/L (desorbed)	12.00	12.66	57.28	-	-	-	-	-	18.06
Na$^+$-500 mmol/L (as-formed)	12.60	13.08	59.54	-	0.48	-	-	0.05	14.32
Na$^+$-500 mmol/L (desorbed)	12.32	12.98	59.35	-	0.14	-	-	-	15.13
K$^+$-500 mmol/L (as-formed)	12.15	12.65	58.79	-	-	0.41	-	0.08	15.63
K$^+$-500 mmol/L (desorbed)	12.31	13.07	59.86	-	-	-	-	-	14.76

Mg^{2+}-200 mmol/L (as-formed)	10.21	10.85	48.92	-	-	-	1.06	0.95	28.00
Mg^{2+}-200 mmol/L (desorbed)	12.25	12.87	57.94	-	-	-	-	-	16.94

3.3. The effects of additives on the morphology of gypsum

Micrographs of the formed gypsum crystals revealed that in the additive-free system, short (4-6 µm) and thin (2-2.5 µm) gypsum crystals formed (Fig. 4a, 5a,b and S6a,b). In contrast, the crystals from the additive-containing solutions were markedly longer and narrower (Fig. 4b, 5b, S6a,b). For example, in the presence of 500 mmol/L Li^+ the end-product gypsum crystals were ~200% longer and ~50% narrower compared with the additive free crystals.

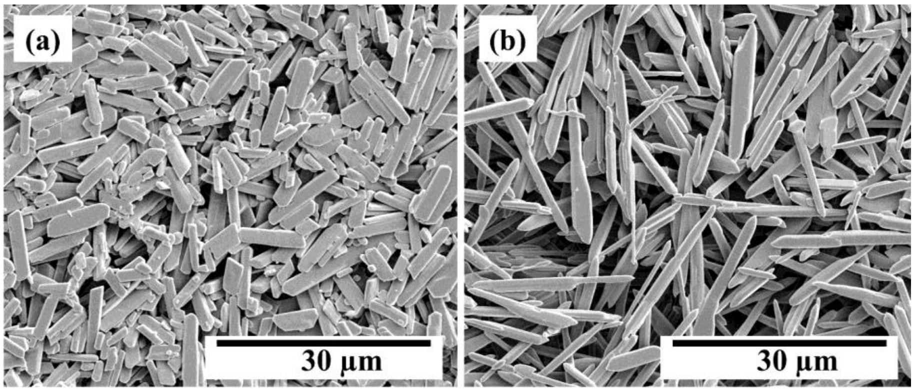

Fig. 4. SEM micrograph of the end-product gypsum crystals in (a) the additive-free system; (b) the presence of 500 mmol/L Li^+ (for morphologies of gypsum crystals precipitated in the presence of K^+, Na^+ and Mg^{2+} see Figs S5).

This is clearly visible in the gypsum crystals grown in the presence of Li^+ and Mg^{2+} where the length of the resulting crystals was almost double, while the widths slightly decreases compared to the additive-free system (Fig. 5a,b and Figs S6a,b).

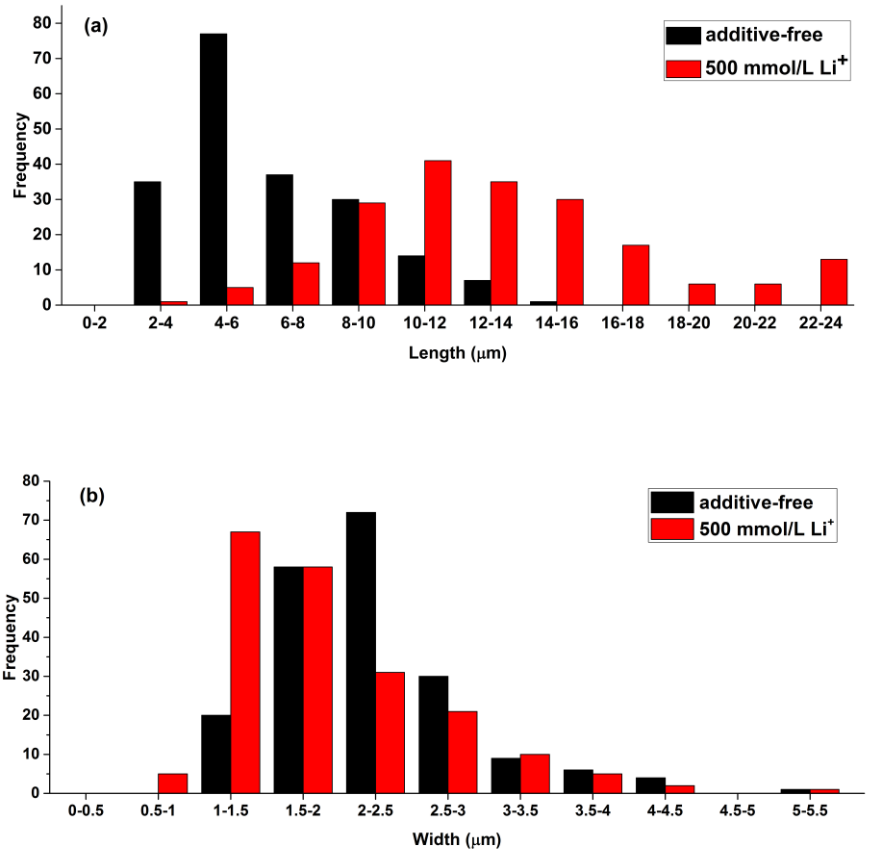

Fig. 5. Particle size analysis of gypsum crystals precipitated from solution containing 500 mmol/L Li^+ after 200 min (a) length of the crystals; (b) width of the crystals (the particles size analysis of the gypsum crystals precipitated in the presence of 500 mmol/L K^+, 500 mmol/L Na^+ and 200 mmol/L Mg^{2+} are in the supporting information Fig. S6a, b).

In addition, the tips of the growing gypsum crystals differed (Fig. 6a-e; S7-10), with the additive-free crystals having flat tips. For example, in the presence of Li^+ the tips were broader and thicker and in these crystals spiral growth and macro-steps were also obvious (Fig. 6a-e and Fig S7a-c). Similarly, the gypsum crystals precipitated in the presence of 500 mmol/L Na^+

(Fig. 6c and Fig. S8) and K$^+$ (Fig. 6d and Fig. S9) had uneven tips with micro-steps while the Mg^{2+} modified gypsum crystals had curved tips (Fig. 6e and Fig. S10).

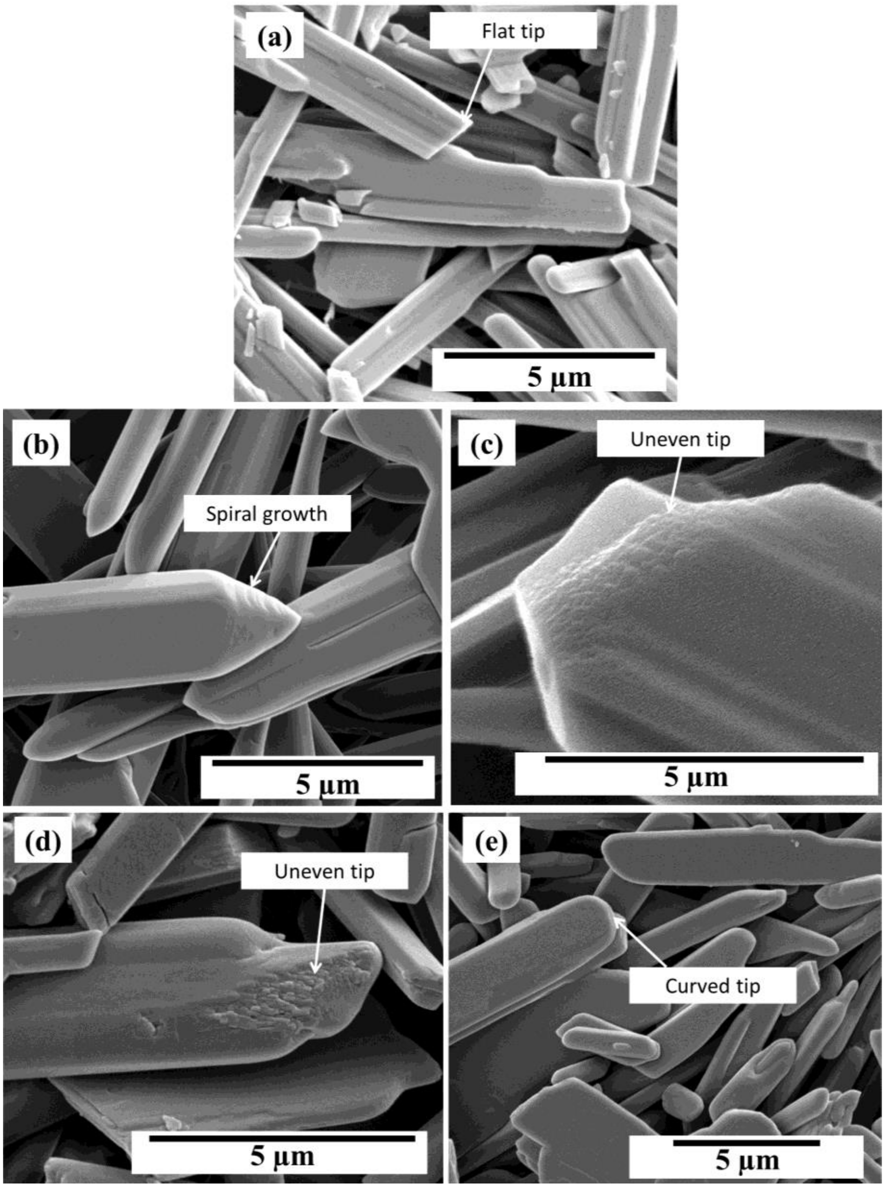

Fig. 6. SEM micrograph of end-product gypsum tips from systems with (a) no additive; (b) 500 mmol/L Li^+ (c) 500 mmol/L Na^+ (d) 500 mmol/L K^+ (e) 200 mmol/L Mg^{2+}.

4. Discussion

4.1. Crystallisation kinetics: role of additives

We used the change in turbidity induction times in the absence and presence of the additives as a proxy to evaluate the effects they have on the nucleation and growth of gypsum. Our data showed a clear increase in induction time with increasing additive concentrations, and a decreased in nucleation and growth kinetics in the order $K^+ < Na^+ < Li^+ < Mg^{2+}$ (Figs. 1a-c). Therefore, it is important to assess if the additives also affected the nucleation and growth mechanisms.

The increase in ionic strength (IS) with increasing the additive concentrations from 50 mmol/L to 500 mmol/L metal invariably resulted in a decrease in the activities of $SO_4^{2-}$and Ca^{2+} and this affected the solubility of gypsum and delayed precipitation (Fig. 1a-c). This is a well-known process in the $CaSO_4$ system Sun et al., 2015; Sverjensky et al., 1997; Tanji, 1969; Zhang et al., 2013. Specially, at high additive ion concentrations, and thus high ionic strengths (IS = 1 mol/L and 0.716 mol/L for 500 mmol/L monovalent cations and 200 mmol/L Mg^{2+} containing solutions, respectively), for example SO_4^{2-}can be present as ion pairs or charged complexes with sodium (Jiang et al., 2013). Such complexes further decrease the activity of free SO_4^{2-} and $CaSO_4^0$ ion pairs. In our study, the additive-sulfate ion-paring strength increased in the order of $K^+ < Na^+ < Li^+ < Mg^{2+}$ ($[KSO_4]^- < [NaSO_4\ ]^- < [LiSO_4]^- < [MgSO_4^0]$) Elgquist and Wedborg, 1978; Jiang et al., 2013; Leaist and Goldik, 2001; Reardon, 1975. As such this likely explains our observation that Mg^{2+} decreased the nucleation rate and increased the solubility of the gypsum crystals more than the monovalent cations. However, it is important to note that the observed order in which these ions affected the induction time and crystallisation kinetics ($K^+ < Na^+ < Li^+ < Mg^{2+}$) is different to what was predicted from the saturation indices calculated by PhreeqC ($Na^+ < Li^+ < K^+ < Mg^{2+}$; Table S3). This indicates that the solubility data in the presence of these ions in the databases (specially for monovalent ions) may need to be re-measured.

Once nucleation is overcome, most often the rate-limiting step for crystal growth is determined by cation desolvation (Dove and Czank, 1995). The increase in hydration enthalpy for $K^+ < Na^+ < Li^+ < Ca^{2+} < Mg^{2+}$ reveals that in our system the divalent Mg^{2+} ion (a *chaotrope*) with the highest hydration enthalpy and water residence time Kerisit and Parker, 2004, by far outcompetes the monovalent ions as it limits crystal growth more effectively. Among the monovalent ions, Li^+ (a *chaotrope*) retained its water longer than Na^+ and K^+ (*kosmotropes*) (Sakuma and Kawamura, 2011).

This is similar to the inhibitory order for the precipitation of calcium oxalate monohydrate as shown by Farmanesh et al., (2015) or for barium sulfate Kowacz et al., (2007).

4.2. Surface adsorption and/or structural incorporation

Our results (Fig. 2, 3 and S3) revealed that all the tested inorganic additives adsorbed onto the surfaces of the gypsum crystals and that among them the cations with more negative hydration enthalpies (Li^+ and Mg^{2+}) had the highest surface adsorption affinity (Table 1). This behaviour can be explained by the water "structure making-structure breaking" model (Gierst et al., 1966). According this model, an ion and a surface exerting similar structural effects on their surrounding water, are attracted entropically to each other. Gypsum has a negative heat of immersion (Singh and Middendorf, 2007), thus, Li^+ and Mg^{2+} will bind stronger to its surface compared to Na^+ and K^+. In addition, equal adsorption (in atomic percentage) of Mg^{2+} and Li^+

(Table 1) despite the more than 2 fold lower concentration of Mg^{2+} (200 mmol/L) than Li^+ (500 mmol/L) further supports this mechanism. Similar behaviours (i.e., higher surface adsorption of Li^+ than Na^+ and K^+) has been reported for TiO_2 Bourikas et al., 2001, α-Al_2O_3 Johnson et al., 1999.

Our data (Table 1 and Fig. S4) also showed a high adsorption affinity of Cl^- on the as-formed gypsum crystals precipitated in the presence of Li^+ and Mg^{2+} but only trace amount of Cl^- on the gypsum crystals formed in the presence of Na^+ and K^+. Sakuma and Kawamura (2011) used molecular dynamics modelling and suggested that cations co-adsorb with chloride on muscovite surfaces. In addition, Rahnemaie et al., (2006), documented that in the goethite-solution double layer Cl^- was closer to the surface than the other ions, and that Li^+ and Na^+ were at the intermediate position of the double layer and K^+ was at the largest distance.

Our observations are in agreement with these previous reports for the monovalent ions Li^+, Na^+ and K^+, but we evidenced further the role of Li^+ and Mg^{2+} in co-adsorbing the chloride ion. This is further supported by the fact that, neither on the surfaces of the as-formed additive-free gypsum crystals nor in all the post desorption gypsum crystals Cl^- was detected by XPS (Table 1 and Fig. S4). This is despite the fact that in all initial solutions used for precipitating gypsum crystals, calcium chloride was a major source of Cl^- in all solutions (200 mmol/L). Moreover, in the samples where Li^+ and Mg^{2+} ions and chloride were determined to be adsorbed to the gypsum surfaces (Table 1), the atomic percentage of the adsorbed Cl^- was in a ratio close to 1:1 with the adsorbed Li^+ and Mg^{2+}. This suggest that Li^+ and Mg^{2+} likely adsorbed onto the gypsum surfaces as chloride ion-pairs or complexes such as $LiCl(H_2O)_4$ for Li^+ (Sobolewski & Domcke, 2005) and $[MgCl(H_2O)_M]^+$ for Mg^{2+} (Siokou et al., 2003). For Li^+ this is supported by the fact that the binding energies for Li 1s and Cl $2p_{3/2}$ at 55.8 eV and 198.5 eV, are the same as the binding energies of these two ions in LiCl (REF WILL BE INSERTED).

It is also worth mentioning that compared with the additive-free gypsum crystals, the Li^+ and Mg^{2+} surface adsorption via sulfate binding shifted the S $2p_{3/2}$ toward higher binding energies by 0.2 eV and 0.49 eV for Li^+ and Mg^{2+}, respectively (Fig. S11). This shift was not observed for the adsorbed Na^+ or K^+, which indicates their low surface adsorption. Hou et al. (2014) reported S $2p_{3/2}$ binding energy variations related to Mg^{2+} association with hydrothermally synthesised calcium sulfate hemihydrate crystals. They attributed this shift to the partial substitution of Ca^{2+} with Mg^{2+} in the calcium sulfate hemihydrate (bassanite) structure and the higher electronegativity of Mg^{2+} (1.39) with respect to Ca^{2+} (1.00), which explained the higher binding energy between Mg^{2+} and S compared to those between Ca^{2+} and S.

Analysing the post desorption gypsum crystals revealed that only Na^+ became partly (max 25%) incorporated into the gypsum structure. Such an incorporation likely happened through substitution of Na^+ for Ca^{2+} specially as Na^+ has the closest ionic radius (1.16 Å) to Ca^{2+} (1.12 Å) compared to the other studied cations (Li^+ = 0.92 Å, K^+ = 1.52 Å and Mg^{2+} = 0.89 Å). Therefore, in gypsum it is likely that Ca^{2+} became substituted by 2 Na^+ ions with one of the Na^+ ions occupying the interstitial positions in the water layer Freyer et al., 1999; Kushnir, 1980.

We are the first to show that when gypsum crystals grown in solutions containing low to high concentrations of monovalent and divalent ions, the prime interaction is through adsorption and that structural incorporation is only a minor effect for Na^+. Previous studies (Kushnir, 1982) reported that Sr^{2+}, Mg^{2+}, Na^+, and K^+ ions present in seawater brines became partitioned into growing gypsum crystals, but no determination whether the partitioning was because of the surface adsorption or structural incorporation is available. Recently, Wang and Meldrum (2012) showed that gypsum crystals synthesised from experimental solutions containing 200 mmol/L Mg^{2+} contained a small, but measurable amount (0.4% mol) of Mg^{2+} in their structure. Similarly, Ahmed et. al. (2014) suggested from XRD analysis of the shift in d-spacing of the gypsum (020) peak, that Mg^{2+} become incorporated into the structure and suggested that this occurred by Mg^{2+} substituting for Ca^{2+}. Based on the same approach they suggested that Na^{+} did not incorporate into the gypsum structure (Ben Ahmed et al., 2014). In our current work, although we observed a similar shift towards lower 2theta in the gypsum (020) peak position as a function of Mg^{2+} concentration (Fig S12), we assert that this is more a function of inherent differences in crystallization paths and not due to the presence of the magnesium ion during gypsum growth. This is because we clearly documented, by two complementary approaches (ICP-MS/ICP-OES analyses of pre- and post-desorption digests and XPS analyses of pre- and post- desorption crystal surfaces), that only <25% of Na^{+} became incorporated into the gypsum structure, while all other ions, even at high concentrations, were solely adsorbed to the growing gypsum crystal surfaces. There, they affected both the growth kinetics and the shapes of the resulting gypsum crystals.

4.3. Morphological modification

The selective adsorption of additives onto the growing gypsum crystals inhibited their growth along specific directions and thus modified their shapes (Fig. 4 and S5). It is not surprising that such inhibition and consequent shape modifications affect most often particular crystal faces and this depends on the attachment energies of the crystal faces Schmidt and Ulrich, 2012. Recently, Massaro et al (2011) demonstrated theoretically that for gypsum, there is a higher site density (Ca^{2+} and SO_4^{2-}) on the (021) planes compared to the fully hydrated (020) planes. Furthermore, the higher surface energy of the (021) faces compared to the (020) faces will affect additives adsorption more Massaro et al., 2011. This is in line with our observations that show that the preferential adsorption of ions happened onto the (021) faces and this favoured growth along the (020) face resulting in the preferential elongation of this face (Fig 4, S5 and S13). In the presence of additives (specially Li^+ and Mg^{2+}) the resulting elongated gypsum crystals was accompanied by a corresponding decrease in the crystal widths (Fig 5 and S6). Furthermore, the presence of additives also affected the growth mechanisms. The spiral growth we have observed for gypsum crystals grown in the presence of additives, together with uneven crystal tips and the presence of growth steps on the crystal surfaces (Fig 6 and S7-10) also confirm the role of additives in gypsum crystal growth. Such observations have not been reported before for mono and divalent ions but similar growth macro-steps have been reported for gypsum crystals grown in the presence of acrylic polymers (Montagnino et al., 2011).

5. Conclusion

With this study we have quantitatively documented the effects that alkali and alkaline earth metals have on the crystallisation of gypsum. The additives increased the time needed for its precipitation to be initiated in the other of $K^+ < Na^+ < Li^+ < Mg^{2+}$. In all cases, gypsum was the sole precipitated phase after 200 minutes and the additives did not cause any phase transformation even at high salt concentrations (500 mmol/L). The combination of ICP-MS / ICP-OES of digested as-formed and post-desorbed digested gypsum crystals together with XPS analyses of the surfaces of these solids revealed that Li^+, K^+ and Mg^{2+} only adsorbed on the surfaces of the gypsum crystals, while small fraction of associated Na+ (max 25%) became structurally incorporated. Growing in the presence of all additives resulted in elongated gypsum crystals, with the change in aspect ratio compared to the additive free system being most prominent in the presence of Li^+ and Mg^{2+} because of their higher surface adsorption affinities.

Supplementary information

The following materials are found in the Supplementary information: Figures S1-13 and Tables S1-3.

Acknowledgements

This study was supported by a Marie Curie grant from the European Commission in the framework of the MINSC ITN (Initial Training Research network), Project number 290040. The authors would like to thank the Cohen Laboratories in the School of Earth and Environment, and the Leeds Electron Microscopy and Spectroscopy Centre (LEMAS) for help and access to instruments during the course of this study.

References

Abràmoff, M. D., Magalhães, P. J. & Ram, S. J. 2004. Image processing with ImageJ. *Biophotonics international,* 11**,** 36-42.

Ben Ahmed, S., Tlili, M. M., Amami, M. & Ben Amor, M. 2014. Gypsum Precipitation Kinetics and Solubility in the NaCl–MgCl2–CaSO4–H2O System. *Industrial & Engineering Chemistry Research,* 53**,** 9554-9560.

Bourikas, K., Hiemstra, T. & Van Riemsdijk, W. 2001. Ion pair formation and primary charging behavior of titanium oxide (anatase and rutile). *Langmuir,* 17**,** 749-756.

Dove, P. M. & Czank, C. A. 1995. Crystal chemical controls on the dissolution kinetics of the isostructural sulfates: Celestite, anglesite, and barite. *Geochimica et Cosmochimica Acta,* 59**,** 1907-1915.

Elgquist, B. & Wedborg, M. 1978. Stability constants of NaSO 4−, MgSO 4, MgF+, MgCl+ ion pairs at the ionic strength of seawater by potentiometry. *Marine Chemistry,* 6**,** 243-252.

Farmanesh, S., Alamani, B. G. & Rimer, J. D. 2015. Identifying alkali metal inhibitors of crystal growth: a selection criterion based on ion pair hydration energy. *Chemical Communications,* 51**,** 13964-13967.

Freyer, D., Reck, G., Bremer, M. & Voigt, W. 1999. Thermal behaviour and crystal structure of sodium-containing hemihydrates of calcium sulfate. *Monatshefte für Chemie/Chemical Monthly,* 130**,** 1179-1193.

Gierst, L., Vandenberghen, L., Nicolas, E. & Fraboni, A. 1966. Ion pairing mechanisms in electrode processes. *Journal of The Electrochemical Society,* 113**,** 1025-1036.

Hamdona, S. K. & Al Hadad, U. A. 2007. Crystallization of calcium sulfate dihydrate in the presence of some metal ions. *Journal of Crystal Growth,* 299**,** 146-151.

Hasson, D., Addai-Mensah, J. & Metcalfe, J. 1990. Filterability of gypsum crystallized in phosphoric acid solution in the presence of ionic impurities. *Industrial & engineering chemistry research,* 29**,** 867-875.

Hoang, T. A., Ming Ang, H. & Rohl, A. L. 2011. Investigation into the effects of phosphonic inhibitors on the formation of calcium sulfate scales. *Desalination and Water Treatment,* 29**,** 294-301.

Jiang, G., Fu, H., Savino, K., Qian, J., Wu, Z. & Guan, B. 2013. Nonlattice Cation-SO42–Ion Pairs in Calcium Sulfate Hemihydrate Nucleation. *Crystal Growth & Design,* 13**,** 5128-5134.

Johnson, S. B., Scales, P. J. & Healy, T. W. 1999. The binding of monovalent electrolyte ions on α-alumina. I. Electroacoustic studies at high electrolyte concentrations. *Langmuir,* 15**,** 2836-2843.

Kerisit, S. & Parker, S. C. 2004. Free energy of adsorption of water and metal ions on the {1014} calcite surface. *Journal of the American Chemical Society,* 126**,** 10152-10161.

Kowacz, M., Putnis, C. & Putnis, A. 2007. The effect of cation: anion ratio in solution on the mechanism of barite growth at constant supersaturation: role of the desolvation process on the growth kinetics. *Geochimica et Cosmochimica Acta,* 71**,** 5168-5179.

Kruger, A., Focke, W. W., Kwela, Z. & Fowles, R. 2001. Effect of ionic impurities on the crystallization of gypsum in Wet-Process Phosphoric Acid. *Industrial & Engineering Chemistry Research,* 40**,** 1364-1369.

Kushnir, J. 1980. The coprecipitation of strontium, magnesium, sodium, potassium and chloride ions with gypsum. An experimental study. *Geochimica et Cosmochimica Acta,* 44**,** 1471-1482.

Leaist, D. G. & Goldik, J. 2001. Diffusion and ion association in concentrated solutions of aqueous lithium, sodium, and potassium sulfates. *Journal of solution chemistry,* 30**,** 103-118.

Mao, X., Song, X., Lu, G., Sun, Y., Xu, Y. & Yu, J. 2014. Effects of Metal Ions on Crystal Morphology and Size of Calcium Sulfate Whiskers in Aqueous HCl Solutions. *Industrial & Engineering Chemistry Research,* 53**,** 17625-17635.

Massaro, F. R., Rubbo, M. & Aquilano, D. 2011. Theoretical equilibrium morphology of gypsum (CaSO4· 2H2O). 2. The stepped faces of the main [001] zone. *Crystal Growth & Design,* 11**,** 1607-1614.

Montagnino, D., Costa, E., Massaro, F., Artioli, G. & Aquilano, D. 2011. Growth morphology of gypsum in the presence of copolymers. *Crystal Research and Technology,* 46**,** 1010-1018.

Rabizadeh, T., Peacock, C. L. & Benning, L. G. 2014. Carboxylic acids: effective inhibitors for calcium sulfate precipitation? *Mineralogical Magazine,* 78**,** 1465-1472.

Rahnemaie, R., Hiemstra, T. & van Riemsdijk, W. H. 2006. A new surface structural approach to ion adsorption: Tracing the location of electrolyte ions. *Journal of colloid and interface science,* 293**,** 312-321.

Reardon, E. 1975. Dissociation constants of some monovalent sulfate ion pairs at 25. deg. from stoichiometric activity coefficients. *The Journal of Physical Chemistry,* 79**,** 422-425.

Sakuma, H. & Kawamura, K. 2011. Structure and dynamics of water on Li+-, Na+-, K+-, Cs+-, H 3 O+-exchanged muscovite surfaces: a molecular dynamics study. *Geochimica et Cosmochimica Acta,* 75**,** 63-81.

Sayan, P., Titiz-Sargut, S. & Avcı, B. 2007. Effect of trace metals on reactive crystallization of gypsum. *Crystal Research and Technology,* 42**,** 961-970.

Schmidt, C. & Ulrich, J. 2012. Morphology prediction of crystals grown in the presence of impurities and solvents—an evaluation of the state of the art. *Journal of Crystal Growth,* 353**,** 168-173.

Sun, J., Wang, L. & Yu, G. 2015. Effects of Na, Ca, Mg, and Al Chloride Salts on Dissolution and Phase Stability of Calcium Sulfate Dihydrate in Aqueous Solutions at 278.15 K to 308.15 K. *Journal of Chemical & Engineering Data*.

Sverjensky, D., Shock, E. & Helgeson, H. 1997. Prediction of the thermodynamic properties of aqueous metal complexes to 1000 C and 5 kb. *Geochimica et Cosmochimica Acta,* 61**,** 1359-1412.

Tanji, K. K. 1969. Solubility of gypsum in aqueous electrolytes as affected by ion association and ionic strengths up to 0.15 M and at 25. deg. *Environmental Science & Technology,* 3**,** 656-661.

Yang, L., Wu, Z., Guan, B., Fu, H. & Ye, Q. 2009. Growth rate of α-calcium sulfate hemihydrate in K–Ca–Mg–Cl–H 2 O systems at elevated temperature. *Journal of Crystal Growth,* 311**,** 4518-4524.

Zhang, Y., Yang, Z., Guo, D., Geng, H. & Dong, C. 2013. Effect of chloride salts and bicarbonate on solubility of CaSO 4 in aqueous solutions at 37 C. *Procedia Environmental Sciences,* 18**,** 84-91.